

1 Noise in Brillouin Based Information Storage

2 OSCAR A. NIEVES^{1,*}, MATTHEW D. ARNOLD¹, MIKOŁAJ K.
3 SCHMIDT², MICHAEL J. STEEL² AND CHRISTOPHER G. POULTON¹

4 ¹ School of Mathematical and Physical Sciences, University of Technology Sydney, 15 Broadway, Ultimo
5 NSW 2007, Australia. ² Department of Physics and Astronomy, Macquarie University, North Ryde NSW
6 2109, Australia.

7 *oscar.a.nievesgonzalez@student.uts.edu.au

8 **Abstract:** We theoretically and numerically study the efficiency of Brillouin-based opto-acoustic
9 data storage in a photonic waveguide in the presence of thermal noise and laser phase noise.
10 We compare the physics of the noise processes and how they affect different storage techniques,
11 examining both amplitude and phase storage schemes. We investigate the effects of storage time
12 and pulse properties on the quality of the retrieved signal, and find that phase storage is less
13 sensitive to thermal noise than amplitude storage.

14 © 2021 Optical Society of America under the terms of the [OSA Open Access Publishing Agreement](#)

15 1. Introduction

16 Stimulated Brillouin scattering (SBS) is an opto-acoustic process that results from the coherent
17 interaction between two counter-propagating optical fields and an acoustic wave inside an optical
18 waveguide [1–5]. In backward SBS, a pump field at frequency ω_1 is injected at one end of
19 the waveguide, and a counter-propagating field at the Brillouin Stokes frequency $\omega_2 = \omega_1 - \Omega$,
20 where Ω is the Brillouin frequency shift, is injected at the other; the interaction of these two
21 fields creates a strong acoustic wave at frequency Ω . When the Stokes power is comparable in
22 size to the pump power, the pump energy can be completely depleted and some of it transferred
23 to the acoustic field, along with its amplitude and phase information. A recent application
24 of this effect is opto-acoustic memory storage (see Fig. 1): an optical data pulse at the pump
25 frequency interacts with an optical “write” pulse (at the Stokes frequency), creating an acoustic
26 hologram where the original data is temporarily stored [6–8]; an optical “read” pulse at the Stokes
27 frequency can then be used to regenerate the original data pulse. Brillouin-based opto-acoustic
28 information storage has been demonstrated experimentally in fibres [6] as well as more recently
29 in on-chip experiments [7–12], with storage times ranging up to 40 ns [12]. Opto-acoustic
30 storage, however, will inevitably be limited by noise, which exists because of the presence of
31 thermal phonons in the waveguide, as well as being an inherent feature of the lasers used in the
32 data and read/write pulses. At room temperatures, it is known that thermal noise significantly
33 degrades the quality of Brillouin processes [13–18], and it can be expected that it will also
34 place limits on information *retrieval efficiency* in Brillouin storage experiments, measured as
35 the amount of power that can be retrieved from the acoustic field after a certain time. This has
36 been experimentally measured [6, 11], however while noise has been observed as a feature of
37 these experiments, it is not yet clear how noise impacts the accuracy of the information retrieval.
38 Furthermore, most studies (except, notably, [10]) have focused on amplitude encoded storage, in
39 which bits of information are stored in individual pulses. Alternatively, phase encoded storage
40 may offer higher storage efficiency and be less sensitive to noise. A quantitative understanding of
41 the impact of noise on the storage of both amplitude and phase information is needed for the
42 further development of practical Brillouin-based storage devices.

43 In this paper, we apply our previous theoretical [18] and numerical [19] models to the
44 simulation of Brillouin storage in the presence of thermal noise. These studies focused on the
45 noise properties of optical pulses in the case of SBS amplification, with the pump containing

46 a lot more power than the input Stokes seed. Here, we investigate the effect of noise on both
 47 amplitude and phase storage of information, by using a small pump power and a large Stokes
 48 seed power. We quantify the retrieval efficiency and accuracy in the form of the packet error rate
 49 (PER) of 8-bit sequences. We find that phase storage offers a significant improvement in the
 50 duration with which information can be stored without degradation due to thermal noise. We
 51 examine this effect in more detail by computing the effect of thermal noise on the amplitude and
 52 phase of a phase-encoded signal, and find that although the variance in amplitude and phase
 53 increases at the same rates, the phase information is more robust to noise in accordance with the
 54 additive-white-Gaussian-noise (AWGN) model of discrete communication theory.

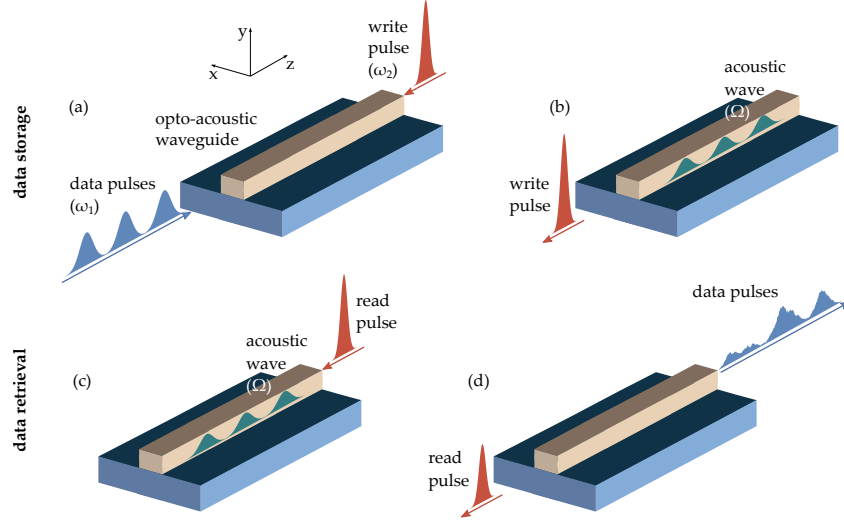


Fig. 1. Illustration of the opto-acoustic storage achieved via SBS, neglecting the effects of noise, and using amplitude shift-keying (amplitude storage). Storage process in (a) and (b): data pulses are depleted by the write-pulse, exciting an acoustic wave inside the waveguide, with some energy gained by the write-pulse. Retrieval process in (c) and (d): a read-pulse interacts with the acoustic wave, both become depleted and the energy is used to regenerate the original sequence of data pulses. The retrieval efficiency is limited by the acoustic lifetime of the phonons.

55 2. Numerical simulation of noise

56 2.1. Brillouin coupled mode equations

We consider a waveguide of length L oriented along the z coordinate axis, in which an optical data stream propagates in the positive z direction. The interaction between the two optical fields and the acoustic field can be described by the coupled system [18, 19]

$$\frac{\partial a_1}{\partial z} + \frac{1}{v} \frac{\partial a_1}{\partial t} + \frac{1}{2} \alpha a_1 = i \omega_1 Q_1 a_2 b^*, \quad (1)$$

$$\frac{\partial a_2}{\partial z} - \frac{1}{v} \frac{\partial a_2}{\partial t} - \frac{1}{2} \alpha a_2 = i \omega_2 Q_2 a_1 b, \quad (2)$$

$$\frac{\partial b}{\partial z} + \frac{1}{v_a} \frac{\partial b}{\partial t} + \frac{1}{2} \alpha_{ac} b = i \Omega Q_a a_1^* a_2 + \sqrt{k_B T} \alpha_{ac} R(z, t). \quad (3)$$

57 where $a_1(z, t)$ and $a_2(z, t)$ are the envelope fields of the data pulse (pump) and read/write pulse
 58 (Stokes) respectively, which correspond to mode fields with frequency/wavenumber $(\omega_{1,2}, k_{1,2})$.

59 $b(z, t)$ is the acoustic envelope field for the mode with frequency/wavenumber (Ω, q) . All
60 envelope fields have units of $\text{W}^{1/2}$. In these equations the optical group velocity is given
61 by $v > 0$ and the acoustic group velocity is denoted $v_a > 0$. α and α_{ac} are the optical and
62 acoustic loss coefficients respectively (in units of m^{-1}). The coefficients $Q_{1,2,a}$ represent the
63 coupling strength of the SBS interaction, which depend on the optical and acoustic modes of the
64 waveguide [20]; from local conservation of energy, we have $Q_1 = -Q_2^*$ and $Q_a = Q_2^*$ [21]. These
65 parameters are related to the SBS gain parameter g_0 (with units of $\text{m}^{-1}\text{W}^{-1}$), via the expression
66 $Q_2 = \sqrt{g_0\Gamma/(4v_a\omega_2\Omega)}$, where $\Gamma = v_a\alpha_{\text{ac}} = 1/\tau_a$ is the rate of decay of the phonons. In deriving
67 Eq. (1)–(3) we have assumed the phase matching conditions $\Omega = \omega_1 - \omega_2$ and $q = k_1 - k_2$.

68 The thermal noise is represented by a zero-mean space-time white noise function, with
69 auto-correlation function given by $\langle R(z, t)R(z', t') \rangle = \delta(z - z')\delta(t - t')$. The parameter $k_B T \alpha_{\text{ac}}$
70 is the strength of the thermal noise, which arises from the fluctuation-dissipation theorem [18].
71 The functions describing the data stream and the read-write pulses are given by $a_{\text{data}}(t)$, $a_{\text{read}}(t)$
72 and $a_{\text{write}}(t)$, which describe the values of the optical envelopes at $z = 0$ (data) and $z = L$
73 (read/write). To incorporate phase noise from the lasers used to generate these fields, the envelope
74 fields at the ends of the waveguide are specified by stochastic boundary conditions, namely
75 $a_1(0, t) = a_{\text{data}}(t)e^{i\phi_1(t)}$ for the data pulse and $a_2(L, t) = [a_{\text{read}}(t) + a_{\text{write}}(t)]e^{i\phi_2(t)}$. The
76 random phase terms $\phi_{1,2}$ are statistically uncorrelated Brownian motions described by

$$\phi_j(t) = \sqrt{2\pi\Delta\nu_L} \int_{-\infty}^t dW(t), \quad (4)$$

77 where $dW(t)$ is a standard Wiener increment [22], and $\Delta\nu_L$ is the laser's intrinsic linewidth [19].

78 In non-storage SBS setups [18, 19] the pump has higher input power P_{p0} than the Stokes P_{s0}
79 and thus behaves as an amplifier. However, in the case of Brillouin storage, we require $P_{p0} \ll P_{s0}$
80 so that the read/write pulse can completely deplete the pump, which contains the data to be stored.
81 Optimum storage requires two conditions on the read/write pulse. First, the read/write pulses
82 must be at least as short in duration as the shortest data pulse. Second, the pulse area for the
83 read/write pulse, defined as [6, 23]

$$\Theta_w = \sqrt{\frac{g_0 v}{8\tau_a}} \int_{-\infty}^{\infty} a_{\text{read/write}}(t) dt, \quad (5)$$

84 must obey the condition $\Theta_w = (m + 1/2)\pi$ where $m = 0, 1, 2, \dots$. This is because once
85 the data pulse is depleted completely, the transfer of energy reverses and the data pulse is
86 regenerated [23–25]. The dependence of the pulse-area on τ_a may seem deceptive at first, but
87 since g_0 is also dependent on τ_a these two effects cancel out.

88 The storage efficiency tells us how effective the storage system is, and may be defined as the
89 ratio of the total output data power $|a_{\text{out}}(t)|^2$ to the total input data power $|a_{\text{data}}(t)|^2$ [10]:

$$\eta_{\text{sto}} = \frac{\int_0^{\tau_{\text{data}}} \langle |a_{\text{out}}(t)|^2 \rangle dt}{\int_0^{\tau_{\text{data}}} \langle |a_{\text{data}}(t)|^2 \rangle dt}, \quad (6)$$

90 where $\langle X(t) \rangle = \frac{1}{N} \sum_{n=1}^N X_n(t)$ is the ensemble average of a function $X(t)$ over N independent
91 runs, and τ_{data} is the duration of the data train. Because the acoustic wave decays in time at a rate
92 $1/\tau_a$, η_{sto} decreases with longer storage times, reducing the efficiency in addition to the effects of
93 noise. We define the storage time τ_{sto} as the temporal delay between the write and read pulses.

94 2.2. Solution to the coupled mode equations

95 We numerically solve Eq. (1)–(3) following the numerical method described in [19]. In brief, we
96 note that the propagation distance of the acoustic wave over the time-scale of the SBS interaction

97 is very small [13]. We therefore apply the limit $\partial_z b \rightarrow 0$ in Eq. (3), and solve the equation
 98 in time via the Green function method [18]. The thermal noise function is simulated starting
 99 at thermal equilibrium at $t = 0$, by drawing random numbers from a steady-state probability
 100 distribution corresponding to an Ornstein-Uhlenbeck process [19,26]. We then substitute the
 101 formal solution $b(z, t)$ into Eq. (1) and (2), and integrate the two equations using a two-step
 102 interactive method: first, the optical fields are translated in space by a distance $\Delta z = v\Delta t$ while the
 103 acoustic field remains stationary [19]. Then, the optical fields at each point in space z are updated
 104 by integrating the equations in time with an Euler-Mayurama scheme [27]. This two-step process
 105 is iterated over multiple time steps to simulate the dynamics of the input pulses.

Parameter	Value	Parameter	Value
Waveguide length L	30 cm	Peak read/write power	0.5–10.5 W
Waveguide temperature T	300 K	Data packets	256
Refractive index n	2.44	Data stream duration τ_{data}	2.44 ns
Acoustic velocity v_a	2500 m/s	Bit duration τ_{bit}	300 ps
Acoustic lifetime τ_a	10.2 ns	Data pulse width τ_1	150 ps
Brillouin shift $\Omega/2\pi$	7.8 GHz	Read pulse width τ_2	100 ps
Brillouin gain parameter g_0	$411 \text{ m}^{-1}\text{W}^{-1}$	Grid size (space) N_z	800
Optical wavelength λ	1550 nm	Grid size (time) N_t	2797
Laser linewidth $\Delta\nu_L$	100 kHz	Step-size Δz	$375 \mu\text{m}$
Peak data power	10 mW	Step-size Δt	3.05 ps
Optical loss α	0.1 dB/cm		

Table 1. Parameters used in this study. Physical parameters correspond to a chalcogenide waveguide [28].

106 For our simulations we use the parameters summarized in Table 1. We assume a high gain
 107 chalcogenide waveguide, of the type used in previous SBS experiments [28]. We store individual
 108 8-bit packets one at a time, consisting of all 256 possible unique 8-bit sequences. Each packet
 109 corresponds to 8 individual pulses in the amplitude storage case, and 4 phases in the phase storage
 110 case, as shown in Fig. 2.

111 It should be noted that the model used here (Eq. (1)–(3)) makes the assumption of the slowly-
 112 varying envelope approximation (SVEA) and rotating-wave approximation (RWA) [18, 21].
 113 Because the optical frequencies used in SBS experiments are typically in the range of a few
 114 hundred THz [1, 29], this means that the pulses simulated must be wider than a few hundred
 115 picoseconds so that these approximations remain valid [30]. Therefore, we limit our simulations
 116 to pulses no shorter than 100 ps, for both for the data and read/write cases. We have chosen
 117 to focus on the storage of 8-bit sequences because they can fit inside a 30 cm chalcogenide
 118 waveguide without being too short to violate the SVEA and RWA, since the acoustic pulses
 119 generated from 300 ps optical bits are approximately 3.7 cm in length.

120 2.3. Data encoding

121 The two storage schemes used in this paper — amplitude and phase storage — are summarized in
 122 Fig. 2. Each bit is defined as having a duration τ_{bit} . For amplitude storage, we encode ones into

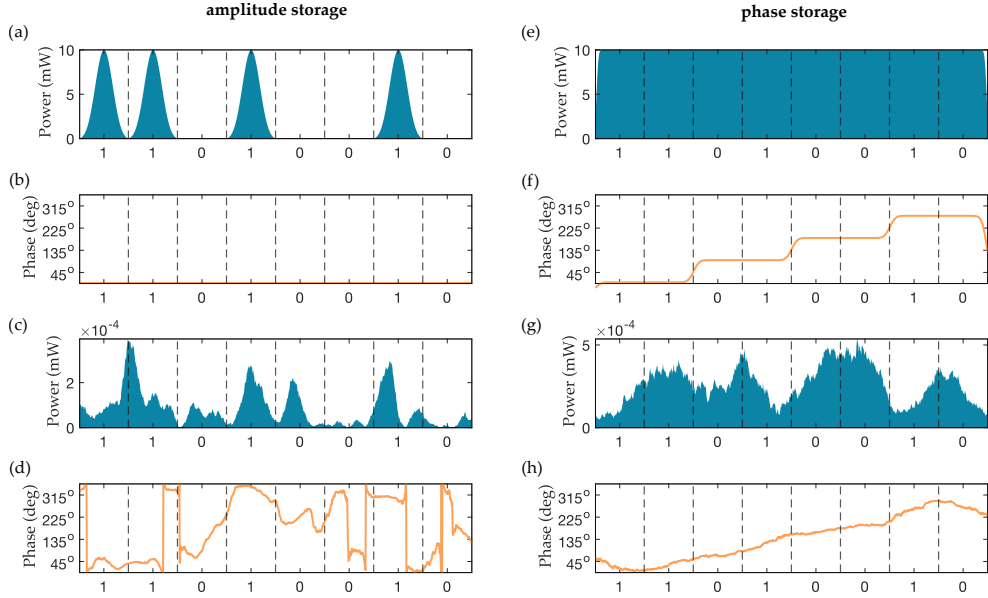


Fig. 2. Illustration of how the 8-bit sequence $\mathbf{x} = 11010010$ is encoded in the numerical simulation. Amplitude storage: (a)–(b) input power and phase, (c)–(d) output power and phase after some storage time. Phase storage: (e)–(f) input power and phase, (g)–(h) output power and phase after some storage time. Here we use thermal noise at $T = 300$ K.

123 Gaussian pulses of the same peak power P_{p0} , while zeros are represented by gaps of duration τ_{bit} .
 124 For phase storage, we use the same scheme as in quadrature phase-shift keying (QPSK) with gray
 125 coding [31], where bit pairs are assigned a unique phase, namely 11 = 45° , 01 = 135° , 00 = 225°
 126 and 10 = 315° . For a given input information packet, we quantify the retrieval accuracy in both
 127 storage schemes via the packet error rate (PER). This is similar to the bit error rate (BER) of
 128 a binary stream, except that we count correct 8-bit packets as opposed to counting individual
 129 correct bits. Therefore, the PER is the ratio of correctly retrieved packets with respect to the
 130 input data, and has a value $0 \leq \text{PER} \leq 1$.

131 In the amplitude storage case, we encode bits=1 into Gaussian pulses of full-width at half-
 132 maximum (FWHM) τ_1 , while bits=0 are represented by gaps of duration τ_{bit} in the data sequence.
 133 By default, we choose all pulses to have a phase of 0° . In the retrieval stage, the output data power
 134 $|a_{\text{out}}(t)|^2$ is separated into equal intervals of length τ_{bit} . We use a dynamic threshold technique:
 135 initially, a threshold power P_{thresh} is set. Then, we record the output power at the center of the bit
 136 period, and a single bit is read as 0 if $|a_{\text{out}}^{(n)}(t)|^2 < P_{\text{thresh}}$ and as 1 if $|a_{\text{out}}^{(n)}(t)|^2 \geq P_{\text{thresh}}$ [32], for
 137 all 256 data packets. This process is repeated for different values of P_{thresh} until the total PER
 138 has been minimized.

139 In the phase storage case, we encode bit-pairs into 4 different phases, as shown in Fig. 3(a),
 140 as part of an analytic smooth rectangular pulse (ASR) [33] with FWHM τ_{data} . We then apply a
 141 Gaussian filter to remove non-physical discontinuities; to emulate the effect of the modulators
 142 used in SBS experiments we have chosen a filter width of 5 GHz, resulting in a smooth phase
 143 transition between the bit-pairs (see Fig. 2(f)). In the retrieval stage, $|a_{\text{out}}(t)|^2$ is separated
 144 into equal intervals of length $2\tau_{\text{bit}}$. We extract the phase from the amplified output signal as
 145 $\phi_{\text{out}}(t) = \tan^{-1}(\text{Im}[a_{\text{out}}(t)]/\text{Re}[a_{\text{out}}(t)])$. As with the case of amplitude storage, we assume
 146 ideal detector conditions and record the phase at the center of the $2\tau_{\text{bit}}$ period, such that if

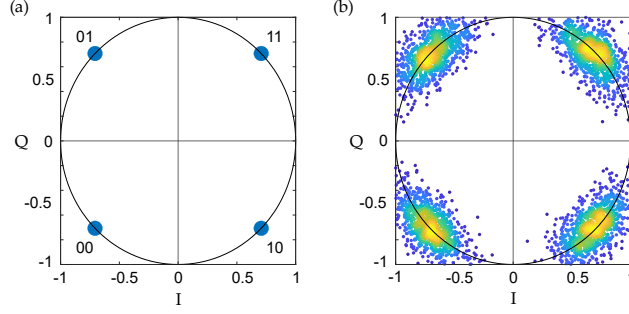


Fig. 3. Constellation diagrams used in phase storage. These plots are done on the complex plane, where the modulus of each point corresponds to the normalized power of the signal, and the argument corresponds to the phase of the signal. (a) ideal system: each point lies at exactly 45° from the horizontal line in either direction, and on the circle of radius 1. (b) Effect of noise in the detected signal: amplitude noise shifts the points in the radial direction, while phase noise shifts the points in the angular direction, and the color scheme shows the regions of higher or lower density of points.

147 $0^\circ < \phi_{\text{out}}(t) < 90^\circ$, we read the output bit-pair as 11, if $90^\circ < \phi_{\text{out}}(t) < 180^\circ$ we read the
 148 bit-pair as 01 and so on. In phase storage, we use another measure of signal integrity based on
 149 the constellation diagram data: let $z_{\text{out}}^{(m)}$ represent a single point on the constellation diagram
 150 corresponding to the m th bit-pair in the binary sequence (such as 00), with magnitude $|z_{\text{out}}^{(m)}|$ and
 151 phase ϕ_z^m . The variances in each can be found via

$$\text{Var} \left[|z_{\text{out}}^{(m)}| \right] = \left\langle |z_{\text{out}}^{(m)}|^2 \right\rangle - \left\langle |z_{\text{out}}^{(m)}| \right\rangle^2, \quad \text{Var} \left[\phi_{\text{out}}^{(m)} \right] = \left\langle \left(\phi_{\text{out}}^{(m)} \right)^2 \right\rangle - \left\langle \phi_{\text{out}}^{(m)} \right\rangle^2. \quad (7)$$

152 3. Results and Discussion

153 3.1. Effect of thermal noise

154 We investigate the effect of varying the read/write pulse peak power between 0.5–10.5 W, while
 155 maintaining a read/write pulse width of 100 ps. We include thermal noise into the waveguide
 156 at 300 K, but neglect the input laser phase noise by setting the laser linewidth $\Delta\nu_L$ to zero. In
 157 the amplitude storage case, we use Gaussian data pulses with 10 mW peak power and pulse
 158 width 150 ps, while in the phase storage case we use a rectangular pulse of duration 2.44 ns, and
 159 phase intervals of duration 600 ps. Each bit of optical information is 300 ps in length for both
 160 amplitude and phase storage. The results of the simulations are shown in Fig. 4. First, we observe
 161 in Fig. 4(a) and (b) that the storage efficiency in both storage schemes is higher as we increase
 162 the peak write pulse power, as the pulse area is lower than the optimum value given by Eq. (5).
 163 Second, we see in Fig. 4(c) and (d) that lower peak write powers lead to increased PER, thus
 164 reducing the maximum storage time achievable in both encoding schemes. This occurs because
 165 at lower peak read/write powers — which also corresponds to the lower storage efficiency regime
 166 — the coherent output data field is less distinguishable from the amplified spontaneous noise
 167 arising from the interaction between the read/write pulse and the thermal background fluctuations
 168 in the waveguide [18, 19]. Consequently, this increases the probability of retrieving the wrong
 169 data sequence at the waveguide output ($z = L$).

170 Similarly, we see an increase in PER in both AS and PS schemes with increasing τ_{sto} , as shown
 171 in Fig. 4(c) and (d). This occurs because in the time between the write and read-process, the
 172 acoustic wave containing the stored information decays at a rate $1/\tau_a$. As τ_{sto} increases, the
 173 acoustic wave gets closer to the background thermal noise, increasing the fluctuations in the

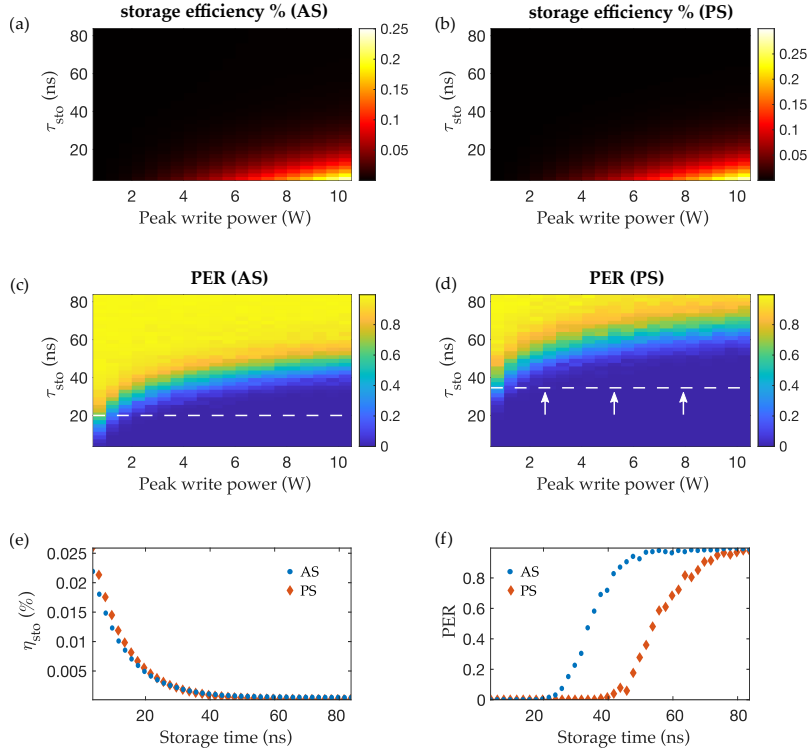


Fig. 4. Simulations of Brillouin storage with thermal noise only, for varying read/write pulse peak power and different storage times in amplitude storage and phase storage. Panels (a) and (b) show the storage efficiency of the two schemes, (c) and (d) the packet error rates, (e) and (f) illustrate the storage efficiency and PER at 3 W peak write power. The dashed horizontal line in (c) and (d) indicates the τ_{sto} at which data packet errors begin to occur, and the arrows in (d) show that this threshold is pushed further back in time.

174 retrieved data field during the read-process. This effect is more clearly illustrated in Fig. 5, where
 175 the constellation points spread out in both radial and angular directions, indicating an increase
 176 in both amplitude and phase noise in the retrieved data field. In Fig. 6 we see that the rate of
 177 increase in the variance of the phase and amplitude of each encoding scheme is the same for the
 178 first 40 nanoseconds. However, in Fig. 4(f) we see that the PER in the phase storage case begins
 179 to increase at longer τ_{sto} compared to the amplitude storage case, suggesting that phase-encoded
 180 data is more robust to thermal noise and hence allows for longer storage times. This occurs
 181 because the phase variations are primarily constrained to a single quadrant on the constellation
 182 plots (as shown in Fig. 5), whereas the amplitude variations reach the noise floor more rapidly.
 183 Consequently, the probability of detecting the wrong bit of information in the amplitude is higher
 184 compared to the phase. This is the same observation that would be expected from the additive
 185 white Gaussian noise (AWGN) model in discrete communication theory, where the probability of
 186 bit error for phase-shift-keying (PSK) is lower than for amplitude-shift-keying (ASK) [34, 35]. In
 187 addition, phase encoding allows the transfer of more bits per symbol, and this means that the
 188 pulse-size constraints imposed by the SVEA and RWA can be further relaxed.

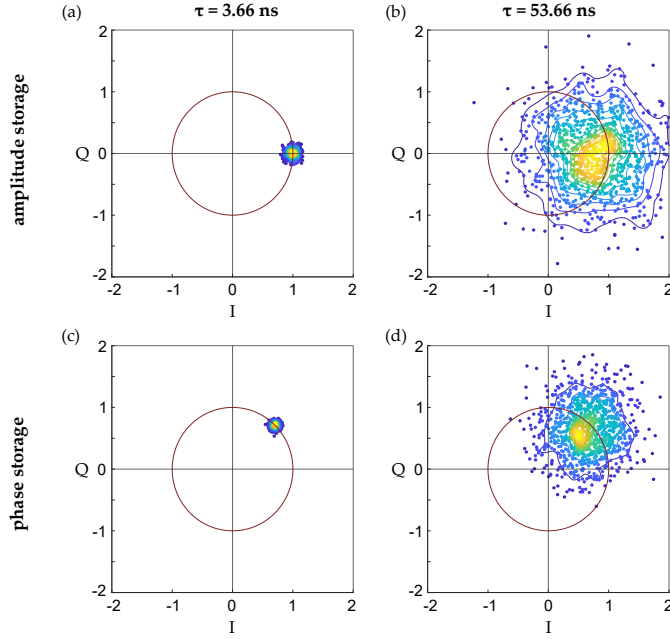


Fig. 5. Constellation diagrams for the thermal noise only case, at 3 W peak write power. (a) and (b) show the amplitude storage plots at two storage times (3.66 ns is the minimum storage time achievable in this configuration) for a binary bit 1, while (c) and (d) show the phase storage plots for a binary bit pair 11.

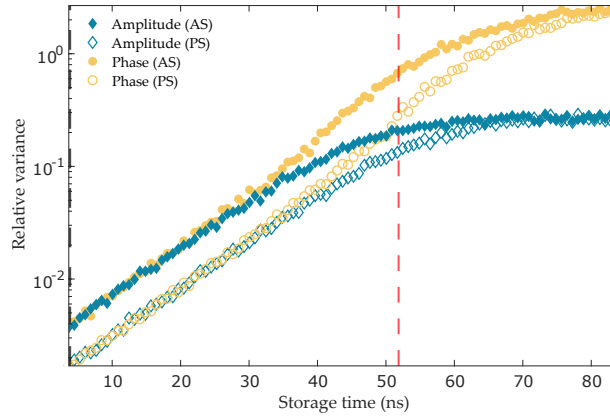


Fig. 6. Relative variance in the amplitude and phase of the constellation data in Fig. 5 as a function of storage time. The dashed lines mark the storage times corresponding to the constellation diagrams in Fig. 5.

189 3.2. Effect of laser phase noise

190 We now investigate the effect of adding input laser phase noise, at a linewidth of 100 kHz, with
 191 the same pulse and thermal noise parameters as before. We generate the phase noise in the data
 192 pulses and read/write pulses independently so they are statistically uncorrelated, but have the
 193 same mean and variance properties. Fig. 7 shows the results for storage efficiency and PER for

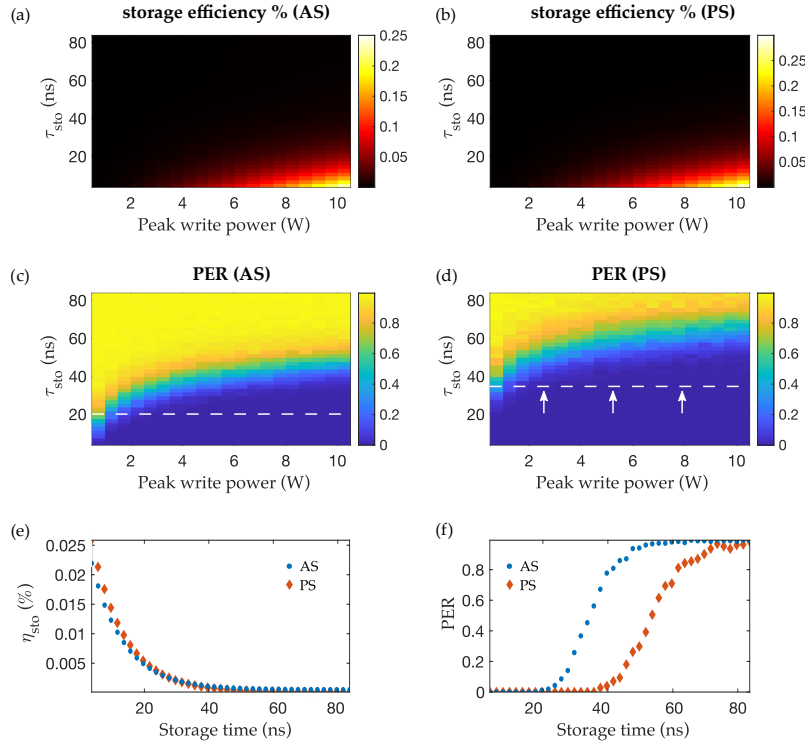


Fig. 7. Simulations of Brillouin storage with both thermal and laser phase noise, for varying read/write pulse peak power and different storage times in amplitude storage and phase storage. Panels (a) and (b) show the storage efficiency of the two schemes, (c) and (d) the packet error rates, (e) and (f) illustrate the storage efficiency and PER at 3 W peak write power. The dashed horizontal line in (c) and (d) indicates the τ_{sto} at which data packet errors begin to occur, and the arrows in (d) show that this threshold is pushed further back in time.

194 both encoding schemes. The plots in Fig. 7(a)–(d) look very similar to Fig. 4(a)–(d), indicating
 195 that laser phase noise does not have a significant impact on the storage efficiency or PER. This is
 196 consistent with previous work on SBS noise in short pulses [19], where it was found that laser
 197 phase noise only has a significant impact on the SBS process when the laser coherence time
 198 ($\tau_{coh} = 1/\pi\Delta\nu_L$) is comparable in magnitude to the SBS interaction time. Next, the constellation
 199 diagram results in Fig. 8 reveal that the input laser phase noise broadens the variance in the
 200 phase of the retrieved data field, making the distribution of constellation points slightly more
 201 elliptical compared to the thermal noise only case. This is also shown in Fig. 9, where the rates
 202 of increase for the amplitude and phase variances still remain approximately the same for the first
 203 40 nanoseconds of storage time. This occurs because at this regime of powers for the data pulses,
 204 the SBS process acts as a linear amplifier, hence the total noise in the retrieved data is a linear
 205 combination of the waveguide thermal noise and the laser phase noise from the inputs.

206 4. Conclusion

207 We have numerically simulated the Brillouin storage of different data packets with thermal and
 208 laser noise, using amplitude storage and phase storage techniques in a photonic waveguide.
 209 Through these computer simulations, we have shown that phase encoded storage allows for longer

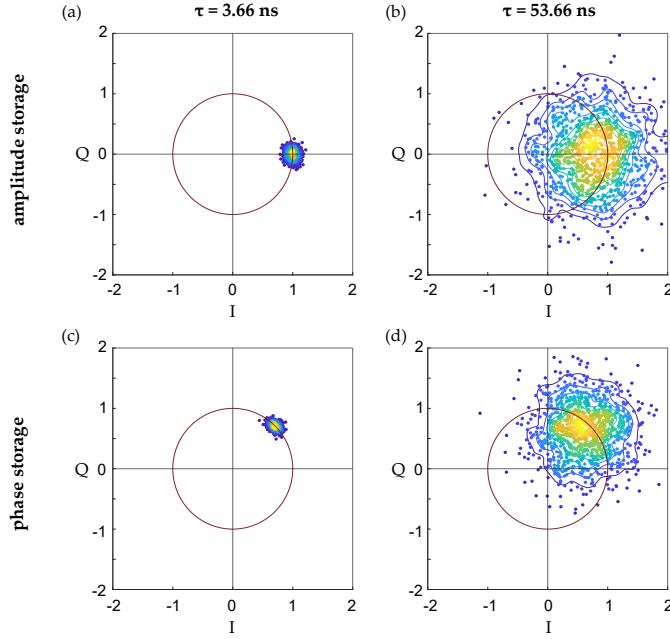


Fig. 8. Constellation diagrams for the thermal noise and laser phase noise case, at 3 W peak write power. (a) and (b) show the amplitude storage plots at two storage times (3.66 ns is the minimum storage time achievable in this configuration) for a binary bit 1, while (c) and (d) show the phase storage plots for a binary bit pair 11.

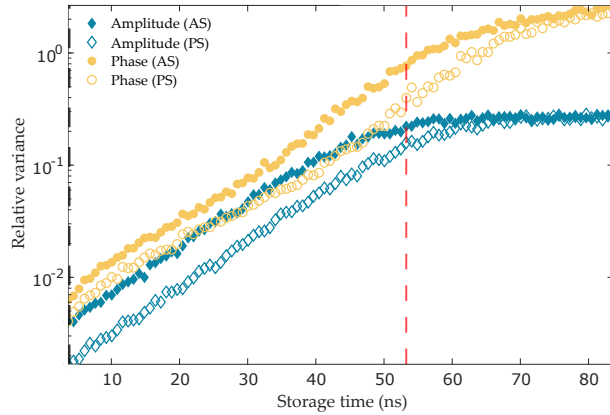


Fig. 9. Relative variance in the amplitude and phase of the constellation data in Fig. 8 as a function of storage time. The dashed lines mark the storage times corresponding to the constellation diagrams in Fig. 8.

210 storage times than amplitude encoded storage. This is because phase encoding is more robust to
 211 noise than amplitude encoding, in accordance with the additive-white-Gaussian-noise model of
 212 discrete communications theory [34]. It is therefore possible to increase Brillouin storage time by
 213 encoding information into the phase of the data field, without having to change the waveguide or
 214 laser properties. Furthermore, because phase storage techniques can encode more bits per symbol
 215 than amplitude storage [31, 34], the pulse size constraints imposed by the SVEA and RWA [30]

216 in these mathematical models can be further relaxed when using phase encoding techniques.

217 Disclosures

218 The authors declare no conflicts of interest.

219 Acknowledgments

220 The authors acknowledge funding from the Australian Research Council (ARC) (Discovery Projects
221 DP160101691, DP200101893), the Macquarie University Research Fellowship Scheme (MQRF0001036)
222 and the UTS Australian Government Research Training Program Scholarship (00099F). Part of the numerical
223 calculations were performed on the UTS Interactive High Performance Computing (iHPC) facility.

224 Data availability Statement

225 Data underlying the results presented in this paper are not publicly available at this time but may be obtained
226 from the authors upon reasonable request.

227 References

- 228 1. B. J. Eggleton, C. G. Poulton, P. T. Rakich, M. J. Steel, and G. Bahl, “Brillouin integrated photonics,” *Nat. Photonics*
229 **13**, 664–677 (2019).
- 230 2. A. Kobayakov, M. Sauer, and D. Chowdhury, “Stimulated Brillouin scattering in optical fibers,” *Adv. Opt. Photonics* **2**,
231 1–59 (2010).
- 232 3. R. Pant, D. Marpaung, I. V. Kabakova, B. Morrison, C. G. Poulton, and B. J. Eggleton, “On-chip stimulated Brillouin
233 scattering for microwave signal processing and generation,” *Laser Photonics Rev.* **8**, 653–666 (2014).
- 234 4. R. W. Boyd, *Nonlinear optics* (Elsevier, 2003).
- 235 5. L. Brillouin, “Diffusion de la lumière et des rayons X par un corps transparent homogène,” *AnPh* **9**, 88–122 (1922).
- 236 6. Z. Zhu, D. J. Gauthier, and R. W. Boyd, “Stored light in an optical fiber via stimulated Brillouin scattering,” *Science*
237 **318**, 1748–1750 (2007).
- 238 7. V. Kalosha, W. Li, F. Wang, L. Chen, and X. Bao, “Frequency-shifted light storage via stimulated Brillouin scattering
239 in optical fibers,” *Opt. Lett.* **33**, 2848–2850 (2008).
- 240 8. M. Merklein, B. Stiller, and B. J. Eggleton, “Brillouin-based light storage and delay techniques,” *J. Opt.* **20**, 083003
241 (2018).
- 242 9. C.-H. Dong, Z. Shen, C.-L. Zou, Y.-L. Zhang, W. Fu, and G.-C. Guo, “Brillouin-scattering-induced transparency and
243 non-reciprocal light storage,” *Nat. Commun.* **6**, 1–6 (2015).
- 244 10. M. Merklein, B. Stiller, K. Vu, S. J. Madden, and B. J. Eggleton, “A chip-integrated coherent photonic-phononic
245 memory,” *Nat. Commun.* **8**, 1–7 (2017).
- 246 11. M. Merklein, B. Stiller, K. Vu, P. Ma, S. J. Madden, and B. J. Eggleton, “On-chip broadband nonreciprocal light
247 storage,” *Nanophotonics* **1** (2020).
- 248 12. B. Stiller, M. Merklein, C. Wolff, K. Vu, P. Ma, S. J. Madden, and B. J. Eggleton, “Coherently refreshing hypersonic
249 phonons for light storage,” *Optica* **7**, 492–497 (2020).
- 250 13. R. W. Boyd, K. Rzaewski, and P. Narum, “Noise initiation of stimulated Brillouin scattering,” *Phys. Rev. A* **42**, 5514
251 (1990).
- 252 14. A. L. Gaeta and R. W. Boyd, “Stochastic dynamics of stimulated Brillouin scattering in an optical fiber,” *Phys. Rev.*
253 *A* **44**, 3205 (1991).
- 254 15. M. Ferreira, J. Rocha, and J. Pinto, “Analysis of the gain and noise characteristics of fiber Brillouin amplifiers,” *Opt.*
255 *Quantum Electron.* **26**, 35–44 (1994).
- 256 16. P. Kharel, R. Behunin, W. Renninger, and P. Rakich, “Noise and dynamics in forward Brillouin interactions,” *Phys.*
257 *Rev. A* **93**, 063806 (2016).
- 258 17. R. O. Behunin, N. T. Otterstrom, P. T. Rakich, S. Gundavarapu, and D. J. Blumenthal, “Fundamental noise dynamics
259 in cascaded-order Brillouin lasers,” *Phys. Rev. A* **98**, 023832 (2018).
- 260 18. O. A. Nieves, M. D. Arnold, M. Steel, M. K. Schmidt, and C. G. Poulton, “Noise and pulse dynamics in backward
261 stimulated Brillouin scattering,” *Opt. Express* **29**, 3132–3146 (2021).
- 262 19. O. A. Nieves, M. D. Arnold, M. J. Steel, M. K. Schmidt, and C. G. Poulton, “Numerical simulation of noise in pulsed
263 Brillouin scattering,” *J. Opt. Soc. Am. B* **38**, 2343–2352 (2021).
- 264 20. B. C. Sturmberg, K. B. Dossou, M. J. Smith, B. Morrison, C. G. Poulton, and M. J. Steel, “Finite element analysis of
265 stimulated Brillouin scattering in integrated photonic waveguides,” *J. Light. Technol.* **37**, 3791–3804 (2019).
- 266 21. C. Wolff, M. J. Steel, B. J. Eggleton, and C. G. Poulton, “Stimulated Brillouin scattering in integrated photonic
267 waveguides: Forces, scattering mechanisms, and coupled-mode analysis,” *Phys. Rev. A* **92**, 013836 (2015).
- 268 22. W. Horsthemke, “Noise induced transitions,” in *Non-equilibrium dynamics in chemical systems*, (Springer, 1984), pp.
269 44–49.

- 270 23. M. Dong and H. G. Winful, "Area dependence of chirped-pulse stimulated Brillouin scattering: implications for
271 stored light and dynamic gratings," *JOSA B* **32**, 2514–2519 (2015).
- 272 24. H. G. Winful, "Chirped Brillouin dynamic gratings for storing and compressing light," *Opt. express* **21**, 10039–10047
273 (2013).
- 274 25. L. Allen and J. H. Eberly, *Optical resonance and two-level atoms*, vol. 28 (John Wiley & Sons., 1975).
- 275 26. G. E. Uhlenbeck and L. S. Ornstein, "On the theory of the Brownian motion," *Phys. review* **36**, 823 (1930).
- 276 27. P. Kloeden and E. Platen, *Numerical Solution of Stochastic Differential Equations* (Springer-Verlag Berlin Heidelberg,
277 1992), 1st ed.
- 278 28. Y. Xie, A. Choudhary, Y. Liu, D. Marpaung, K. Vu, P. Ma, D.-Y. Choi, S. Madden, and B. J. Eggleton, "System-level
279 performance of chip-based Brillouin microwave photonic bandpass filters," *J. Light. Technol.* **37**, 5246–5258 (2019).
- 280 29. C. Wolff, M. Smith, B. Stiller, and C. Poulton, "Brillouin scattering—theory and experiment: tutorial," *JOSA B* **38**,
281 1243–1269 (2021).
- 282 30. J. Piotrowski, M. K. Schmidt, B. Stiller, C. G. Poulton, and M. J. Steel, "Picosecond acoustic dynamics in stimulated
283 Brillouin scattering," *Opt. Lett.* **46**, 2972–2975 (2021).
- 284 31. S. Faruque, *Radio frequency modulation made easy* (Springer, 2017), pp. 69–83.
- 285 32. D. Walsh, D. Moodie, I. Mauchline, S. Conner, W. Johnstone, and B. Culshaw, "Practical bit error rate measurements
286 on fibre optic communications links in student teaching laboratories," in *9th International Conference on Education
287 and Training in Optics and Photonics (ETOP)*, Marseille, France, Paper ETOP021, (2005).
- 288 33. E. Granot, "Propagation of chirped rectangular pulses in dispersive media: analytical analysis," *Opt. Lett.* **44**,
289 4745–4748 (2019).
- 290 34. D. R. Smith, *Digital transmission systems* (Springer science & business media, 2012), pp. 370–381.
- 291 35. D. Bala, "Analysis the probability of bit error performance on different digital modulation techniques over AWGN
292 channel using MATLAB," *J. Electr. Eng. Electron. Control. Comput. Sci.* **7**, 9–18 (2021).